Comparative Finite-Element Assessment of Conventional Steel and SMA–FRP Hybrid Reinforcement in Reinforced-Concrete Beam–Column Joint Configurations

Ms. Payal Maruti Gadiwadd[1], Prof. V. M. Bogar[2]
[1] *PG Schlolar Department of Applied Mechanics, Government College of Engineering Karad*
[2] *Assistant Proffessor Department of Applied Mechanics, Government College of Engineering Karad*

Abstract*—Reinforced-concrete (RC) beam–column joints govern the transfer of axial force, shear and bending moment in moment-resisting frames and frequently become critical under earthquake-induced load reversals. This study presents a comparative three-dimensional finite-element assessment of conventional steel reinforcement and a shape-memory-alloy–fibre-reinforced-polymer (SMA–FRP) hybrid system for three structurally distinct configurations: a cantilever beam, an overhanging beam–column assembly and a floating-column/transfer-beam system. The source models were developed in ANSYS Mechanical using M25 concrete, conventional reinforcing steel, superelastic NiTi SMA properties and homogenised SMA–FRP rebar properties. The reported response quantities were total deformation, equivalent von Mises stress, middle principal stress, equivalent elastic strain and strain energy. Percentage change was recomputed directly from the numerical values to remove a contradictory legacy conclusion embedded in the presentation. For the cantilever case, the hybrid system reduced deformation, von Mises stress, elastic strain and strain energy by 9.18%, 8.44%, 8.88% and 8.15%, respectively. The corresponding reductions for the overhanging case were 9.21%, 8.33%, 9.14% and 9.11%. The floating-column model was the most demanding configuration and exhibited the greatest hybrid benefit: deformation decreased from 20.77 to 16.58 mm (20.17%), von Mises stress from 196.38 to 139.57 MPa (28.93%), elastic strain by 20.02% and strain energy by 20.07%. Middle principal stress remained essentially unchanged (−0.61% to +0.04%), indicating local redistribution rather than a uniform stress reduction. The results support the use of SMA–FRP reinforcement as a response-control strategy at critical joints and discontinuity regions; however, the available dataset contains static response contours rather than complete cyclic hysteresis, residual-drift or mesh-convergence evidence. Consequently, the findings demonstrate improved finite-element response indicators but should not be interpreted as full seismic qualification without cyclic experimental validation.

***Index Terms*—beam–column joint; shape memory alloy; fibre-reinforced polymer; hybrid reinforcement; ANSYS; floating column; seismic resilience**

I. INTRODUCTION

Reinforced-concrete moment-resisting frames rely on beam–column joints to transmit forces between adjoining members while maintaining compatibility of deformation. During strong ground motion, the joint core and adjacent plastic-hinge regions are exposed to high shear stress, bond deterioration, bar slip, stiffness degradation and repeated opening and closing of cracks. Damage in these zones is particularly consequential because brittle joint failure can interrupt the intended strong-column–weak-beam mechanism and trigger storey-level or progressive collapse. Modern seismic design therefore seeks not only adequate strength but also stable cyclic response, controlled damage, limited residual drift and rapid post-earthquake functional recovery.

Conventional reinforcing steel provides high stiffness, established design procedures and substantial inelastic energy absorption. Its principal limitation in highly damaged plastic-hinge regions is the accumulation of permanent strain after yielding. Residual deformation may render a frame uneconomic to repair even when collapse is prevented. Superelastic shape memory alloys (SMAs), especially NiTi alloys, can recover large strains through stress-induced phase transformation and are therefore attractive for self-centering reinforcement. Fibre-reinforced polymer (FRP) bars and composites provide high tensile strength and corrosion resistance but generally have lower elastic modulus, linear-elastic response to rupture and limited inherent ductility. Hybridisation is intended to combine the recoverability of SMA with the strength and durability of FRP while retaining adequate force-transfer capacity.

Previous analytical and experimental work has shown that SMA-containing systems can reduce residual deformation and improve collapse safety, whereas partial FRP–steel hybridisation can enhance durability and cyclic performance when the FRP fraction is appropriately controlled (Billah & Alam, 2012; Zafar & Andrawes, 2015; Nahar et al., 2020; Javan et al., 2023). Recent joint tests further indicate that SMA combined with steel plates or engineered cementitious composites can improve self-centering and delay stiffness deterioration, although full replacement of steel by a lower-modulus SMA system may reduce initial stiffness or strength (Pei et al., 2022; Qian et al., 2022). These observations underline the need for case-specific numerical evaluation rather than assuming that a hybrid material is universally superior.

The present study evaluates three configurations that represent different support and load-path conditions: a cantilever beam, an overhanging beam–column assembly and a floating-column/transfer-beam model. Each configuration is compared using conventional reinforcement and an SMA–FRP hybrid alternative. The reported ANSYS outputs are interpreted in terms of deformation demand, equivalent stress, principal stress, elastic strain and strain energy. Particular attention is given to the floating-column case because interruption of the vertical load path concentrates demand in the transfer member and adjoining joint region.

A publication-oriented data audit was undertaken before interpretation. The presentation contained duplicate literature entries, a material row labelled “geopolymer” with metal-like properties, incomplete geometric/load documentation and one hidden conclusion asserting that conventional steel performed better by approximately 31–33%. That statement is incompatible with every case-wise numerical table, which consistently reports lower deformation, equivalent stress, elastic strain and strain energy for the SMA–FRP model. The present manuscript therefore adopts the case-wise numerical tables as the controlling dataset, transparently records the unresolved inputs and limits the claims to quantities actually available.

II. PROBLEM STATEMENT

RC joints and discontinuity regions may experience concentrated force transfer, severe cracking and permanent deformation under lateral loading. Conventional steel detailing can satisfy strength requirements but may retain significant plastic strain after a severe earthquake, while FRP-only reinforcement may lack ductility and SMA-only reinforcement may reduce stiffness or load capacity because its modulus is lower than that of steel. A technically viable hybrid system must therefore control deformation and stress without creating unfavourable local stress concentrations or compromising the load path.

The specific problem addressed is the absence of a directly comparable numerical assessment of conventional steel and SMA–FRP hybrid reinforcement across three markedly different structural configurations using a common set of response parameters. The cantilever case concentrates flexure at a fixed root, the overhanging case introduces unbalanced moment and support-region joint demand, and the floating-column case creates a discontinuous vertical load path. The study seeks to determine whether the hybrid reinforcement consistently reduces response demand and whether its relative benefit changes with structural irregularity.

III. RESEARCH GAP

- Most published SMA studies emphasise complete frames, bridge columns or specialised self-centering joints; direct case-wise comparisons across support and discontinuity configurations remain limited.
- Hybrid SMA–FRP research commonly focuses on residual drift and cyclic energy dissipation, whereas comparative finite-element evidence for deformation, von Mises stress, elastic strain and

stored strain energy at joint/member level is less consistently reported.
- Floating-column and transfer-beam zones are widely recognised as irregular load paths, yet their interaction with hybrid smart reinforcement is underexplored relative to regular beam–column joints.
- Published studies frequently use different geometry, loading histories and material fractions, making it difficult to isolate how structural configuration affects the benefit of hybrid reinforcement.
- Many numerical investigations do not clearly separate demonstrated static-response improvements from unverified claims regarding self-centering, hysteretic energy dissipation and residual deformation.
- Long-term durability, bond–slip, environmental degradation, prestress loss, constructability and cost of SMA–FRP systems remain insufficiently integrated into numerical performance comparisons.

The present work addresses the first four gaps by evaluating identical response measures for three configurations and by quantifying percentage reductions relative to conventional steel. It addresses the fifth gap by explicitly distinguishing static strain energy from hysteretic energy dissipation and by identifying the additional cyclic data required for full seismic verification.

IV. AIM AND OBJECTIVES

Aim: To evaluate, through comparative three-dimensional finite-element analysis, the response of conventional steel and SMA–FRP hybrid reinforced RC joint/member configurations and to identify the structural case in which hybrid reinforcement provides the greatest demand reduction.
- To compile and critically assess the geometry, reinforcement and material properties reported for the conventional and hybrid finite-element models.
- To model or interpret the cantilever, overhanging and floating-column configurations under their reported support and loading conditions.
- To compare total deformation, equivalent von Mises stress, middle principal stress, equivalent elastic strain and strain energy for conventional and SMA–FRP reinforcement.
- To calculate percentage change relative to conventional steel and rank the three configurations by absolute demand and hybrid improvement.
- To interpret stress/deformation contours in relation to load path, support condition and potential seismic vulnerability.
- To validate the numerical comparison through arithmetic verification and consistency with peer-reviewed experimental and numerical literature, while identifying the data needed for full cyclic validation.

V. LITERATURE REVIEW

The development of hybrid reinforcement for seismic-resilient concrete structures is motivated by the complementary behaviour of steel, SMA and FRP. Steel supplies stiffness and ductile yielding; superelastic SMA supplies recoverable strain and recentering; FRP supplies high tensile strength and corrosion resistance. Billah and Alam (2012) demonstrated at column level that placing SMA in the plastic-hinge region and FRP elsewhere can reduce residual displacement while maintaining useful ductility and energy dissipation. Zafar and Andrawes (2015) extended the concept to moment-resisting frames under sequential mainshock–aftershock records and reported lower residual drifts and reduced damage accumulation for SMA–FRP composite reinforcement.

At joint level, Kabir et al. (2016) synthesised early steel, FRP and SMA hybrid studies and concluded that hybridisation can improve recoverability and durability, but its effectiveness depends strongly on reinforcement location, anchorage and the balance between stiffness and recentering. Nahar et al. (2020) used nonlinear finite-element models, pushover analysis and incremental dynamic analysis to show that SMA-reinforced beam–column joints achieved higher collapse margins than conventional steel-reinforced joints. Abraik (2020) similarly found that SMA-based plastic-hinge strategies improved frame response under sequential seismic hazards by limiting residual damage.

Experimental evidence indicates that neither SMA nor FRP should be treated as a simple one-for-one replacement for steel. Pei et al. (2022) tested self-centering joints and observed that replacement by SMA alone reduced stiffness and capacity, whereas a combined SMA–steel-plate configuration restored strength while improving ductility and self-centering. Qian et al. (2022) reported that SMA bars markedly improved recentering and that engineered cementitious composites improved ductility and energy dissipation; the combined system delayed stiffness degradation. Javan et al. (2023) found that partial GFRP replacement of steel could improve ductility and damping, but high GFRP ratios reduced stiffness and cyclic stability.

FRP strengthening research supports the premise that fibre composites can control joint shear damage and redirect failure away from the joint core. Hashemi and Riahi (2022) demonstrated improved capacity using near-surface-mounted steel bars and CFRP strips. Ong et al. (2022) reviewed confinement-based retrofit methods and identified anchorage, debonding, constructability and the absence of unified design guidance as continuing limitations. Karayannis and Golias (2022) tested full-scale joints strengthened with CFRP ropes, while Golias et al. (2024) reproduced the behaviour using three-dimensional finite-element modelling and reported agreement with full-scale tests.

Recent studies continue to explore combined smart-material and composite systems. Selim et al. (2024) reported that fly-ash concrete joints with hybrid GFRP–steel reinforcement achieved improved load capacity, ductility and energy absorption for an optimum partial GFRP range. Al Ekkawi and El-Hacha (2025) showed that prestressed Fe-SMA plates increased lateral strength, displacement ductility, energy dissipation and recentering of deficient RC columns, with additional benefits from CFRP or UHPFRC confinement. Collectively, the literature supports hybridisation but also shows that its benefit depends on configuration, material fraction, interface behaviour and loading protocol.

Table 1. Representative literature on SMA, FRP and hybrid reinforcement for RC seismic applications.

Author and year	Research topic	Methodology	Major findings	Limitations/research gap
Billah & Alam (2012)	Hybrid SMA–FRP RC columns	Numerical seismic comparison of SMA, FRP, stainless-steel and hybrid reinforcement layouts	Hybrid layouts reduced residual displacement while retaining ductility and energy dissipation	Column-focused; joint-core and bond behaviour not directly evaluated
Zafar & Andrawes (2015)	SMA–FRP reinforced RC frames under sequential hazards	Performance-based frame design and incremental dynamic analysis under mainshock–aftershock sequences	Lower residual drift and damage accumulation with SMA–FRP composite reinforcement	Analytical frame study; material cost and construction details not resolved
Kabir et al. (2016)	Hybrid RC beam–column joints	Critical review of steel, FRP, SMA–steel and SMA–FRP systems	SMA-based hybrids improve recentering and FRP improves durability	Limited standardised test data and design guidance
Nahar et al. (2020)	Collapse safety of SMA RC joints	Nonlinear FE modelling, pushover and incremental dynamic analysis using 20 records	SMA joints achieved higher collapse margins than steel joints	Results depend on constitutive calibration and selected ground motions
Abraik (2020)	SMA RC frames under sequential earthquakes	Nonlinear FE mainshock–aftershock analysis	SMA plastic-hinge strategies reduced residual response and accumulated damage	Frame-level modelling; limited experimental validation

Author and year	Research topic	Methodology	Major findings	Limitations/research gap
Pei et al. (2022)	Self-centering SMA beam–column joints	Four 1/5-scale cyclic tests and OpenSees parametric analysis	SMA alone reduced stiffness/capacity; SMA plus steel plate improved strength, ductility and recentering	Specialised joint detail; scale and anchorage effects
Qian et al. (2022)	SMA–ECC self-centering joints	Five half-scale low-cycle tests plus finite-element parametric study	SMA improved recentering; ECC improved ductility and energy dissipation	Uses ECC rather than FRP and requires specialised material zones
Hashemi & Riahi (2022)	NSM steel/CFRP joint strengthening	Cyclic tests on three strengthening schemes and a control joint	Capacity increased and plastic hinging shifted away from the joint	External retrofit; long-term bond and fire durability remain concerns
Javan et al. (2023)	Hybrid GFRP–steel joints	Five half-scale joints under cyclic lateral and constant axial loading	Partial GFRP replacement improved ductility and damping; high ratios reduced stiffness	No SMA component; limited specimen number
Al Ekkawi & El-Hacha (2025)	Fe-SMA plates with CFRP/UHPFRC confinement	Four deficient RC columns tested under quasi-static cyclic loading	Fe-SMA increased strength, ductility, dissipation and recentering; confinement gave additional gains	Column strengthening rather than internal hybrid joint reinforcement

VI. MATERIALS AND METHODS / RESEARCH METHODOLOGY

6.1 Study design and source-data audit

The study is a comparative finite-element investigation based on the complete numerical data, tables and ANSYS images contained in the source presentation. The conventional steel model is treated as the reference, and the SMA–FRP model is treated as the comparative alternative. Three cases are analysed separately before cross-case ranking. Because raw ANSYS project files, load magnitudes, solver logs and mesh-convergence records were not supplied with the presentation, the manuscript does not reconstruct missing inputs or invent numerical values. Instead, it documents the available properties, reproduces the reported outputs and performs independent arithmetic checks.

Table 2. Data-integrity audit and adopted treatment.

Issue	Observation	Treatment in this manuscript
Contradictory conclusion	A hidden paragraph states that conventional steel is better by 31.47–33.36%, whereas all three case tables show lower response for SMA–FRP.	Case-wise numerical tables control; the unsupported paragraph is excluded.
Analysis scope	Methodology slides refer to cyclic and pushover analysis, but the reported outputs are static structural contours and scalar extrema.	Results are described as finite-element response indicators, not complete cyclic seismic proof.

Issue	Observation	Treatment in this manuscript
Geopolymer property row	The listed E = 200 GPa and strengths of 250/460 MPa resemble metallic reinforcement rather than geopolymer concrete.	Entry is retained only as a data anomaly and not used in interpretation.
Geometry definition	Column 1500 × 230 mm and beam 600 × 230 mm are reported without a complete three-dimensional cross-section convention.	Values are reproduced exactly; unreported thickness/width is not assumed.
Loading and mesh	Load magnitude, axial load ratio, element type, contact, rebar embedding, mesh size and convergence tolerance are absent.	No code-level capacity or mesh-independent validation is claimed.
Material selection	Several FRP fibres and homogenised composite ranges are listed, but the exact hybrid composition used for each result is not identified.	The property envelope is reported; the selected ANSYS material card requires confirmation.

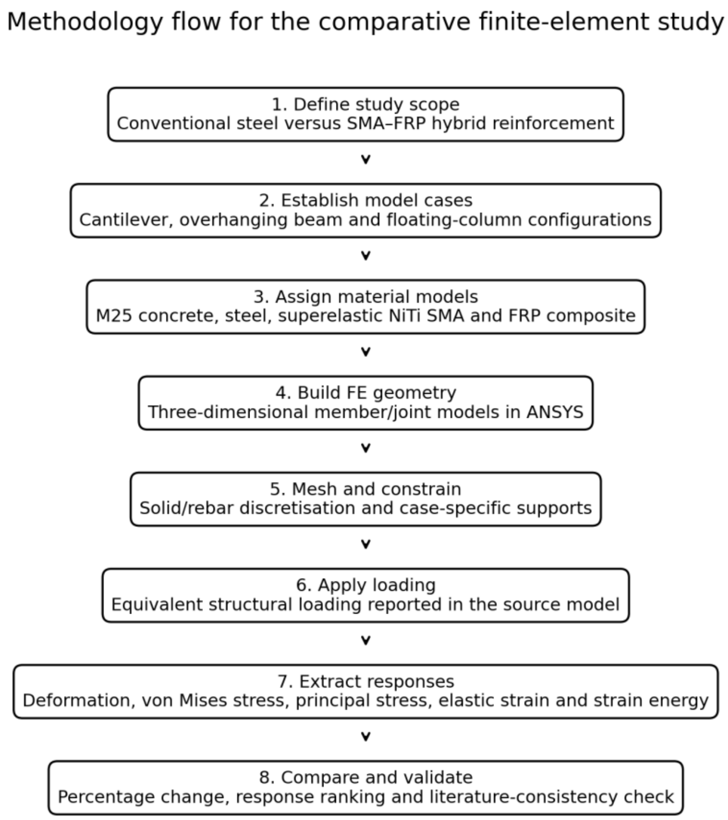

Figure 1. Chronological methodology used to convert the source finite-element study into a reproducible comparative assessment.

6.2 Geometry and reinforcement

The source specimen is presented as a T-shaped RC member/joint model. The vertical member is reported as 1500 × 230 mm and reinforced with thirteen 10 mm bars, while the beam is reported as 600 × 230 mm and reinforced with nine 8 mm bars. The presentation does not explicitly state whether the second dimension is width, depth or a common section thickness; consequently, no sectional area, reinforcement ratio or nominal moment capacity is calculated. This limitation is material because such calculations would otherwise require the complete beam and column cross-sections, clear cover, bar arrangement and shear reinforcement.

Table 3. Reported geometry and reinforcement details.

Component	Reported dimension	Longitudinal reinforcement	Clarification required
Column/vertical member	1500 × 230 mm	13 bars of 10 mm diameter	Full 3D cross-section and tie details not reported
Beam/horizontal member	600 × 230 mm	9 bars of 8 mm diameter	Full 3D cross-section, cover and stirrups not reported
Joint region	T-shaped intersection	Conventional steel or SMA–FRP hybrid reinforcement	Anchorage length, splice and bond model not reported

ANSYS model development and discretisation

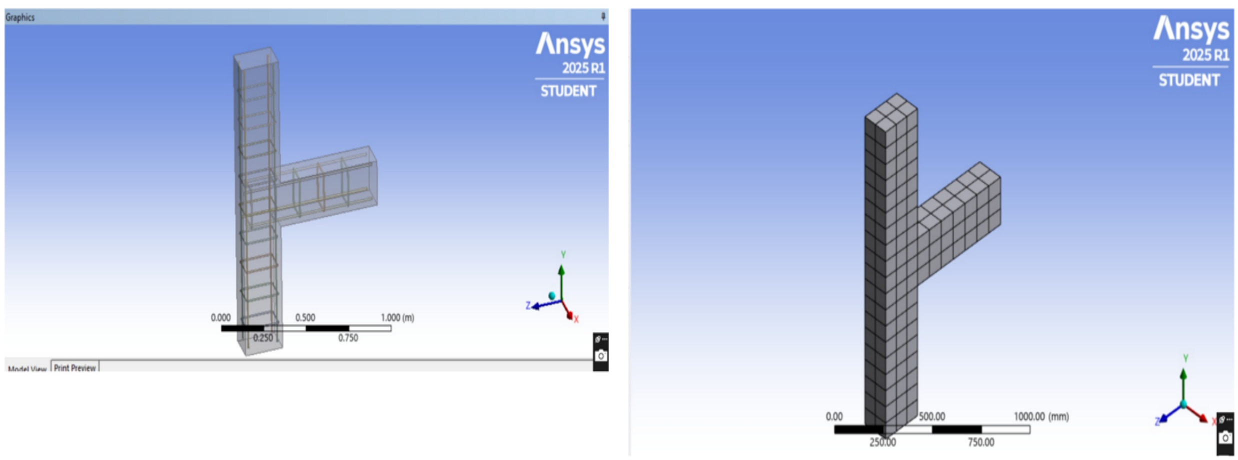

(a) Three-dimensional reinforced-concrete model (b) Meshed T-shaped model

Figure 2. Three-dimensional ANSYS model and representative finite-element mesh reproduced from the source presentation.

6.3 Constituent material properties

M25 concrete and conventional steel form the baseline RC model. The listed concrete modulus of 32.92 GPa is retained as supplied rather than replaced by a code-derived value. Steel is represented by an elastoplastic response with strain hardening, whereas the SMA is intended to represent superelastic forward and reverse phase transformation. FRP is described as linear elastic up to rupture. The presentation also supplies several candidate fibre moduli and a resin modulus, indicating that the hybrid rebar was conceptually homogenised; however, the volume fractions and exact homogenisation procedure are not given.

Table 4. Baseline material properties reproduced from the presentation.

Material	Property	Value
Structural steel	Yield stress	265 MPa
Structural steel	Ultimate tensile strength	500 MPa
Structural steel	Young’s modulus	205 GPa
Structural steel	Poisson’s ratio	0.30
Structural steel	Ultimate tensile strain	0.25
M25 concrete	Compressive strength	25 MPa
M25 concrete	Tensile strength	3.5 MPa

Material	Property	Value
M25 concrete	Young's modulus	32.92 GPa
M25 concrete	Poisson's ratio	0.15
CFRP entry in source table	Compressive yield strength	600 MPa
CFRP entry in source table	Tensile strength	3000 MPa
CFRP entry in source table	Young's modulus	70 GPa
CFRP entry in source table	Poisson's ratio	0.20

Table 5. Reported SMA transformation and FRP constituent properties.

Constituent	Property	Value
NiTi SMA	Austenite Young's modulus	63.50 GPa
NiTi SMA	Forward transformation start stress	365 MPa
NiTi SMA	Forward transformation finish stress	425 MPa
NiTi SMA	Reverse transformation start stress	102 MPa
NiTi SMA	Reverse transformation finish stress	50 MPa
Low-modulus carbon fibre	Young's modulus / ultimate strain	230 GPa / 1.60%
High-modulus carbon fibre	Young's modulus / ultimate strain	370 GPa / 1.00%
S-glass fibre	Young's modulus / ultimate strain	86.7 GPa / 3.20%
E-glass fibre	Young's modulus / ultimate strain	68.9 GPa / 2.00%
Aramid fibre	Young's modulus / ultimate strain	124.1 GPa / 3.00%
Polymer resin	Young's modulus / yield stress	1.57 GPa / 22 MPa

Table 6. Homogenised SMA–FRP composite-rebar properties reported in the presentation.

Composite type	Effective modulus	Peak stress
SMA–FRP benchmark (S7)	14.14 GPa	102.22 MPa
S-glass + SMA (high SMA content)	approximately 14–18 GPa	381.17 MPa
Carbon + SMA hybrid	approximately 16–20 GPa	250–340 MPa

The exact composite type, fibre/SMA volume fractions and selected ANSYS input curve are not stated in the source file.

The recommended ANSYS representation in the presentation uses a multilinear material law with the composite initial modulus, an SMA transformation plateau, an ultimate stress selected from the homogenised composite table and a failure strain governed by FRP rupture. For publication-grade reproducibility, the complete stress–strain points, loading/unloading branches and element-level failure/deletion criteria should be supplied in a future revision.

6.4 Finite-element model, loading and boundary conditions

The images show a three-dimensional solid model and a regular discretisation of the T-shaped member. The methodology proposes nonlinear concrete behaviour capable of cracking and crushing, elastoplastic steel and superelastic SMA. The actual solver screenshots available in the results are consistent with ANSYS Static Structural output. Case-specific restraint and load application were inferred only at the qualitative level from the figures: the cantilever is fixed at one end and loaded towards the free end; the overhanging configuration transfers load through a column/support joint to a projecting beam; and the floating-column configuration introduces a vertical discontinuity above a transfer beam. A constant column axial load and displacement-controlled cyclic loading are discussed in the proposed methodology, but their numerical amplitudes and time histories are absent from the reported results.

Table 7. Model cases and qualitative boundary/load-path characteristics.

Case	Support/load path	Critical zone	Expected governing behaviour
Cantilever beam	One end fixed; free-end action	Fixed face/beam root	Flexural stress concentration at fixed end; maximum deformation at free end
Overhanging beam	Column/support with projecting beam portion	Support and beam–column joint	Unbalanced moment, joint shear and serviceability of the overhang
Floating column	Vertical member terminates on transfer beam	Transfer beam, floating-column base and joint	Load-path discontinuity, local deformation and concentrated transfer demand

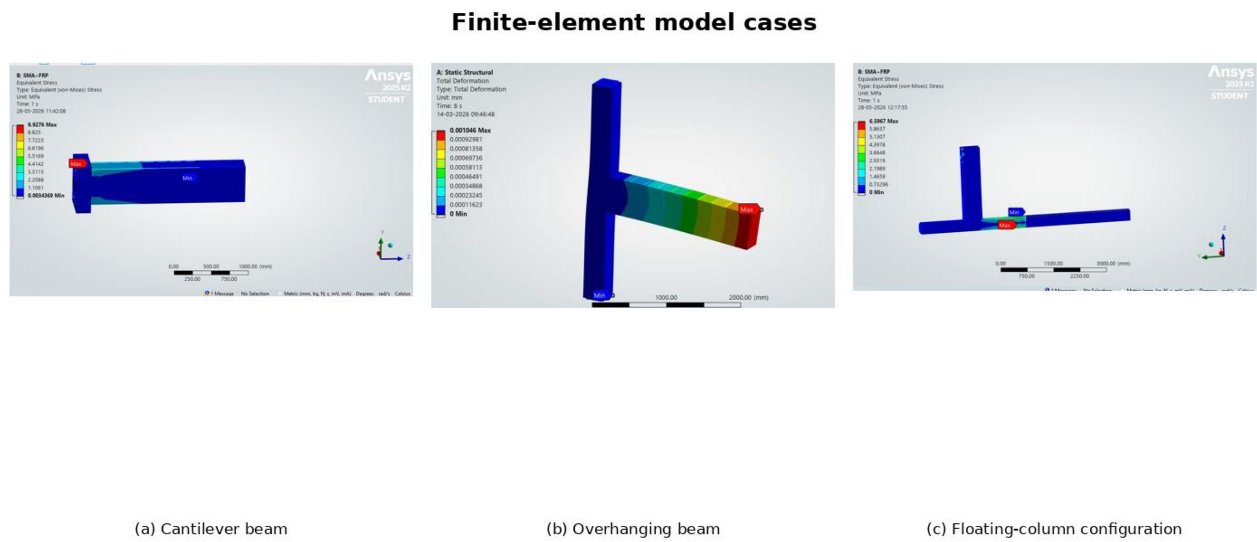

Figure 3. Representative ANSYS model cases: cantilever, overhanging beam–column assembly and floating-column/transfer-beam system.

6.5 Governing response equations and comparison metrics

Equivalent von Mises stress is used as a scalar measure of multiaxial stress intensity. In terms of the principal stresses σ1, σ2 and σ3 (MPa), it is evaluated as:

$$\sigma\_vm = \sqrt{[(\sigma_1 - \sigma_2)^2 + (\sigma_2 - \sigma_3)^2 + (\sigma_3 - \sigma_1)^2] / 2} \quad (1)$$

Here, σ_vm is the equivalent von Mises stress. Although concrete is pressure-sensitive and is not governed by a von Mises yield criterion, the scalar remains useful for consistent comparison of the two model variants and for interpreting reinforcement-related stress fields.

For a linearly elastic response component, the elastic strain tensor is related to stress through the constitutive matrix D, while the total stored strain energy is:

$$\varepsilon^e = D^{-1}\sigma; \quad U = \tfrac{1}{2} \int_v (\sigma : \varepsilon^e)\, dV \quad (2)$$

The elastic strain ε^e is dimensionless, D is the elastic constitutive matrix, V is model volume and U is the strain energy. The source presentation reports U in mJ. In a static analysis, U is stored recoverable energy and must not be equated directly with hysteretic energy dissipation, which requires cyclic load–displacement loops.

The percentage reduction of the hybrid response relative to conventional steel is calculated from the user-specified expression:

$$R = [(X\_ref - X\_hybrid) / X\_ref] \times 100\% \quad (3)$$

X_ref is the conventional-steel value and X_hybrid is the SMA–FRP value. A positive R denotes a reduction; a negative R denotes an increase.

To summarise the four principal response measures (deformation, von Mises stress, elastic strain and strain energy), an average normalised response index is calculated as:

$$I\_avg = (1/n)\, \Sigma[(X\_hybrid,i / X\_ref,i) \times 100], \quad n = 4 \quad (4)$$

A lower index represents a lower average response relative to the conventional model. This index is a descriptive comparison and not a code-defined performance index.

VII. MODEL AND CASE DETAILS

7.1 Cantilever-beam case

The cantilever model develops a clear bending-dominated load path. The fixed support restrains translation and rotation, causing the bending moment, equivalent stress and strain to concentrate at the beam root. Total deformation increases monotonically towards the free end. In earthquake-resistant detailing, this region corresponds to a potential hinge or anchorage-critical zone where concrete confinement, bar development length and interface compatibility of the hybrid reinforcement are decisive.

7.2 Overhanging beam–column case

The overhanging assembly consists of a vertical support/member and a projecting horizontal beam. The support and joint must transfer the unbalanced moment generated by the overhanging portion. The source contours show maximum deformation towards the unsupported end and local stress/strain concentration near the column face. Relative to a pure cantilever, the joint geometry and member intersection create a more complex multiaxial stress state and increase the importance of shear transfer and anchorage through the joint core.

7.3 Floating-column/transfer-beam case

The floating-column configuration introduces a discontinuity because the vertical member terminates on a transfer beam rather than continuing to the foundation. Gravity and lateral actions must therefore be redirected through the transfer member and its connections. The discontinuity creates local stiffness changes and concentrated shear, bending and bearing demand. This case is expected to be particularly vulnerable during earthquakes because lateral drift and vertical load redistribution may act simultaneously, and damage at the transfer joint can compromise multiple upper-storey load paths.

VIII. RESULTS AND DISCUSSION

8.1 Cantilever response

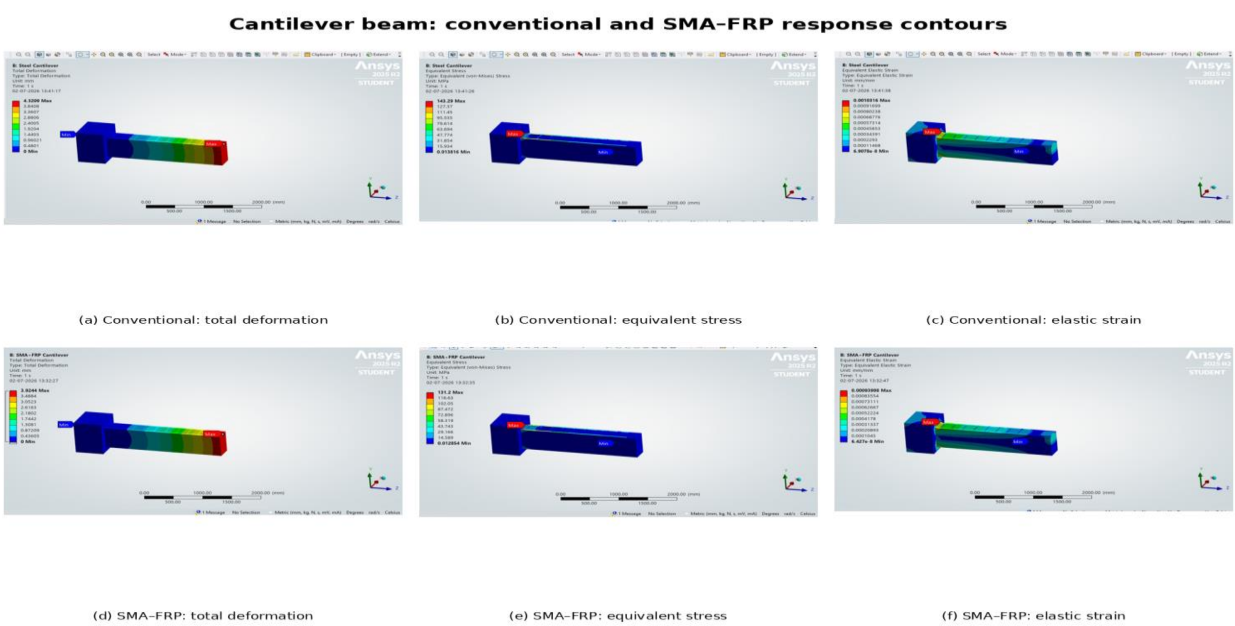

Figure 4. Cantilever-beam contours for conventional steel and SMA–FRP hybrid models: total deformation, equivalent stress and elastic strain.

The deformation contours confirm maximum displacement at the free end and minimum movement at the fixed support. Equivalent stress and elastic strain are concentrated near the fixed face, consistent with the maximum bending moment location. The SMA–FRP model reduces total deformation from 4.3209 to 3.9244 mm, a reduction of 9.18%. Equivalent von Mises stress decreases from 143.29 to 131.20 MPa (8.44%), and equivalent elastic strain decreases from 0.0010316 to 0.00093998 (8.88%). Strain energy falls from 3790.2 to 3481.4 mJ (8.15%).

Middle principal stress increases slightly from 4.5927 to 4.6205 MPa, corresponding to −0.61% by the adopted reduction formula. Because the global deformation and equivalent stress both decline, this small increase is interpreted as local redistribution rather than overall deterioration. The result also demonstrates why a single stress component should not be used alone to judge hybrid performance; joint design should consider the complete principal-stress field and crack-sensitive tensile zones.

8.2 Overhanging-beam response

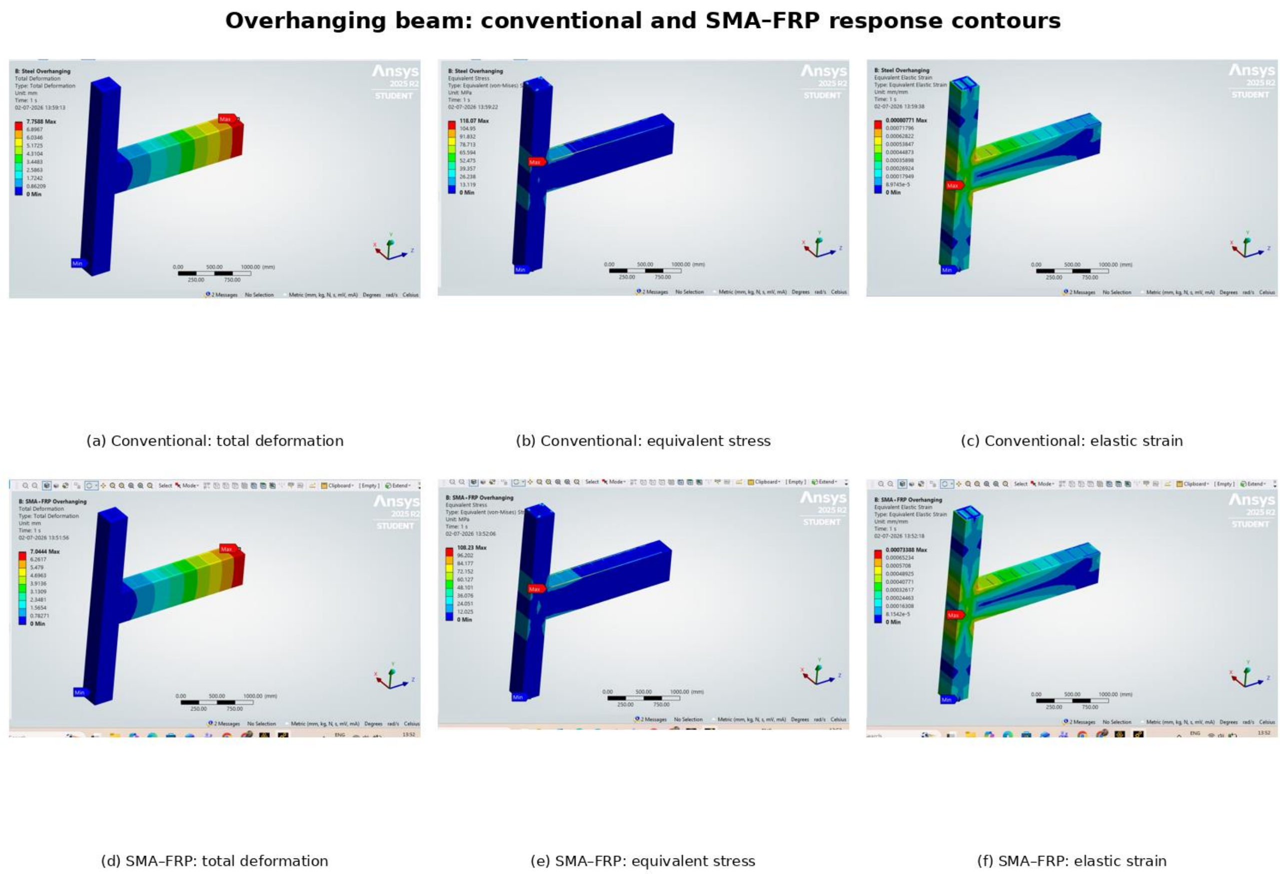

Figure 5. Overhanging beam–column contours for conventional steel and SMA–FRP hybrid models.

The overhanging case shows deformation concentrated in the projecting/free portion and stress concentration near the support and beam–column intersection. The total deformation decreases from 7.7588 to 7.0444 mm, equivalent to 9.21%. Von Mises stress decreases from 118.07 to 108.23 MPa (8.33%), equivalent elastic strain decreases from 0.00080771 to 0.00073388 (9.14%) and strain energy decreases from 9307.3 to 8459.7 mJ (9.11%). These reductions are internally consistent and indicate a moderate response-control effect similar to the cantilever case.

The middle principal stress changes from 9.3419 to 9.3786 MPa, a slight increase of 0.39%. This again points to stress redistribution in the joint/support region. The absolute principal stress is the largest among the three conventional cases, even though the von Mises stress and elastic strain are lower than those of the cantilever and floating-column models. The observation highlights the multiaxial nature of the overhanging joint and the need to check crack orientation, joint shear and bond demand rather than relying only on a scalar equivalent stress.

8.3 Floating-column response

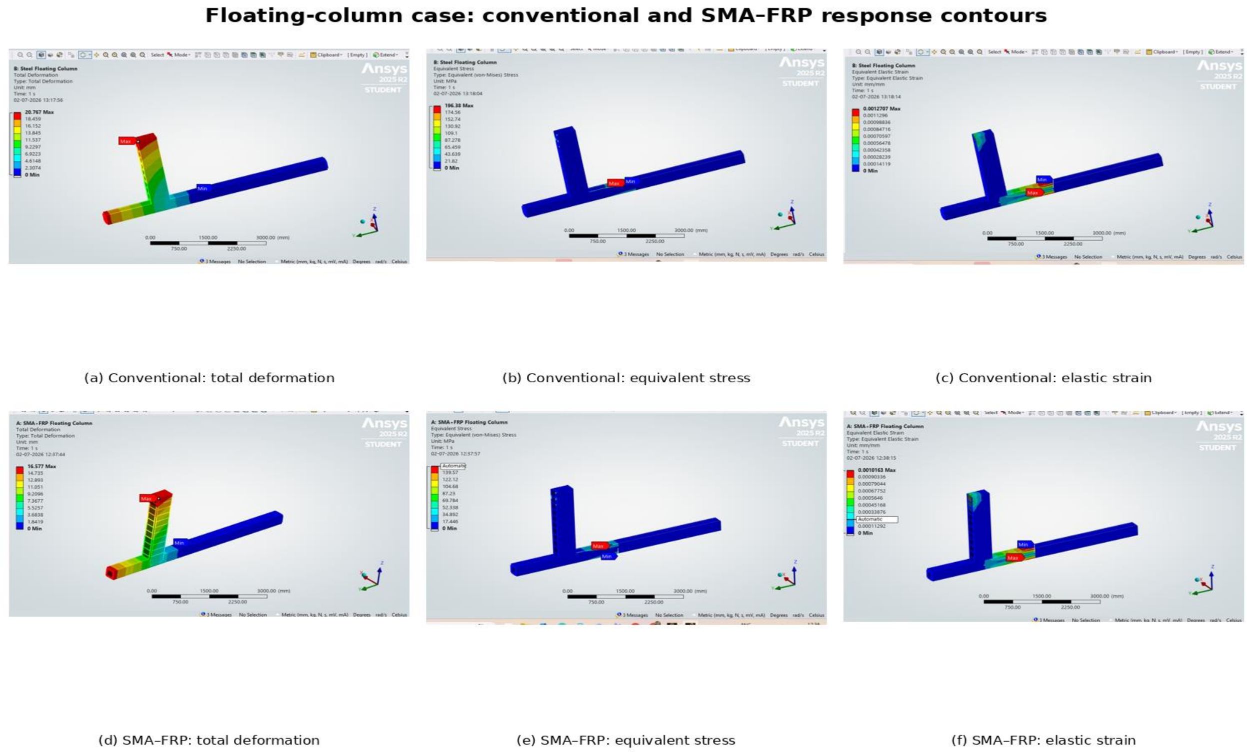

Figure 6. Floating-column/transfer-beam contours for conventional steel and SMA–FRP hybrid models.

The floating-column model produces the largest deformation, von Mises stress, elastic strain and strain energy of all cases. Total deformation decreases from 20.77 to 16.58 mm with the hybrid reinforcement, a reduction of 20.17%. Von Mises stress decreases from 196.38 to 139.57 MPa, giving the maximum single improvement in the study at 28.93%. Equivalent elastic strain decreases from 0.0012707 to 0.0010163 (20.02%), and strain energy decreases from 37,645 to 30,088 mJ (20.07%).

Middle principal stress remains effectively unchanged, decreasing from 7.0542 to 7.0512 MPa (0.04%). The strong reductions in the other four responses suggest that the hybrid system is most beneficial when the structural load path is highly discontinuous and response demand is concentrated. Nevertheless, the hybrid model still records 16.58 mm deformation and 139.57 MPa equivalent stress; therefore, the floating-column arrangement remains the most critical configuration and should not be considered acceptable solely because its relative reduction is large.

Table 8. Complete numerical comparison of conventional and SMA–FRP models.

Case	Response parameter	Conventional	SMA–FRP	Calculated change
Cantilever	Total deformation (mm)	4.3209	3.9244	9.18% reduction
Cantilever	von Mises stress (MPa)	143.29	131.20	8.44% reduction
Cantilever	Middle principal stress (MPa)	4.5927	4.6205	0.61% increase
Cantilever	Equivalent elastic strain	0.0010316	0.00093998	8.88% reduction
Cantilever	Strain energy (mJ)	3790.2	3481.4	8.15% reduction

Case	Response parameter	Conventional	SMA–FRP	Calculated change
Overhanging	Total deformation (mm)	7.7588	7.0444	9.21% reduction
Overhanging	von Mises stress (MPa)	118.07	108.23	8.33% reduction
Overhanging	Middle principal stress (MPa)	9.3419	9.3786	0.39% increase
Overhanging	Equivalent elastic strain	0.00080771	0.00073388	9.14% reduction
Overhanging	Strain energy (mJ)	9307.3	8459.7	9.11% reduction
Floating column	Total deformation (mm)	20.77	16.58	20.17% reduction
Floating column	von Mises stress (MPa)	196.38	139.57	28.93% reduction
Floating column	Middle principal stress (MPa)	7.0542	7.0512	0.04% reduction
Floating column	Equivalent elastic strain	0.0012707	0.0010163	20.02% reduction
Floating column	Strain energy (mJ)	37,645	30,088	20.07% reduction

8.4 Cross-case comparison and performance ranking

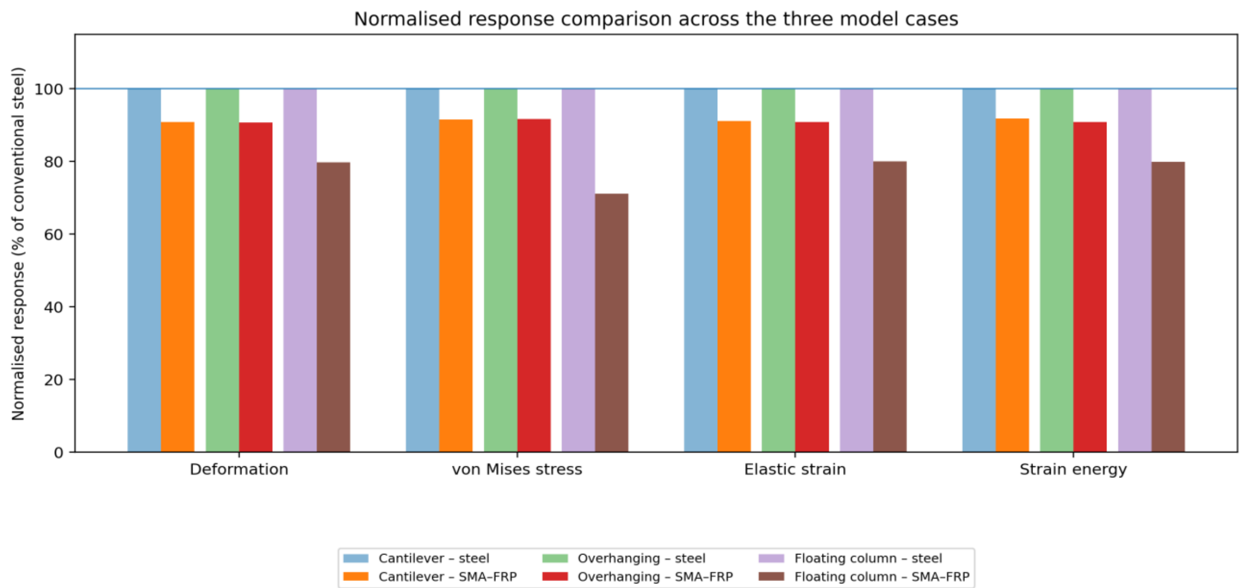

Figure 7. Normalised hybrid response relative to conventional steel (conventional = 100%).

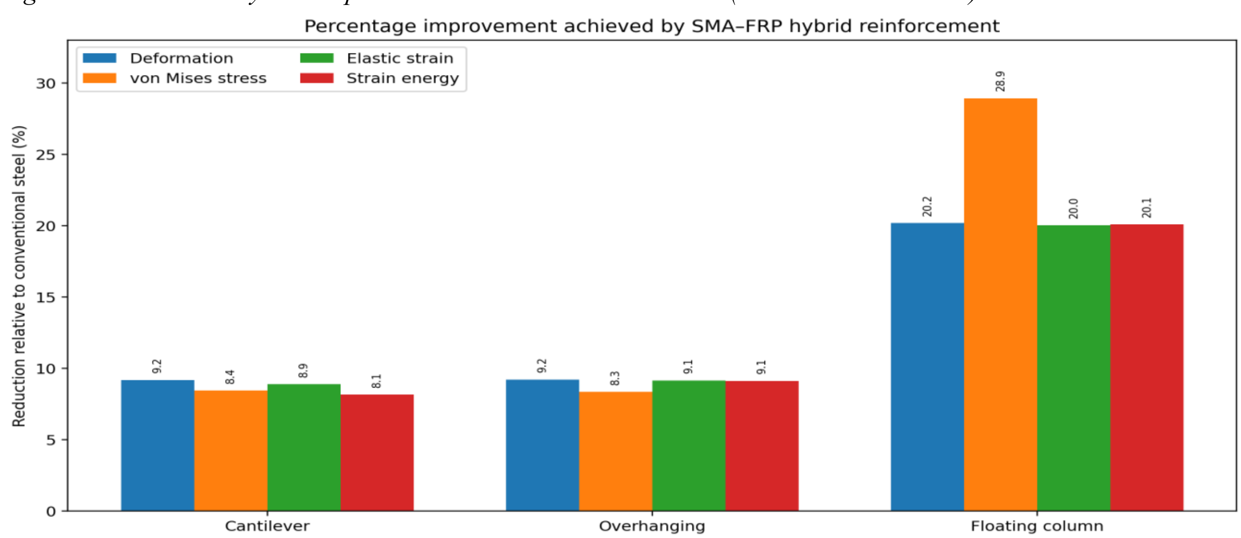

Figure 8. Percentage reduction in the four principal response measures for each case.

The cantilever and overhanging cases show closely grouped improvements. Averaging deformation, von Mises stress, elastic strain and strain energy gives mean reductions of 8.66% and 8.95%, respectively. The floating-column case gives a mean reduction of 22.30%, more than twice the improvement of either regular support case. Across all twelve principal comparisons, the arithmetic mean reduction is 13.30%.

In absolute terms, the floating-column configuration ranks first in severity for deformation, von Mises stress, elastic strain and strain energy for both reinforcement systems. The overhanging case has the largest middle principal stress, while the cantilever lies between the other two cases for equivalent stress and strain. The response ranking is therefore not identical for every measure, but the floating column is clearly the dominant critical case when the combined indicators are considered.

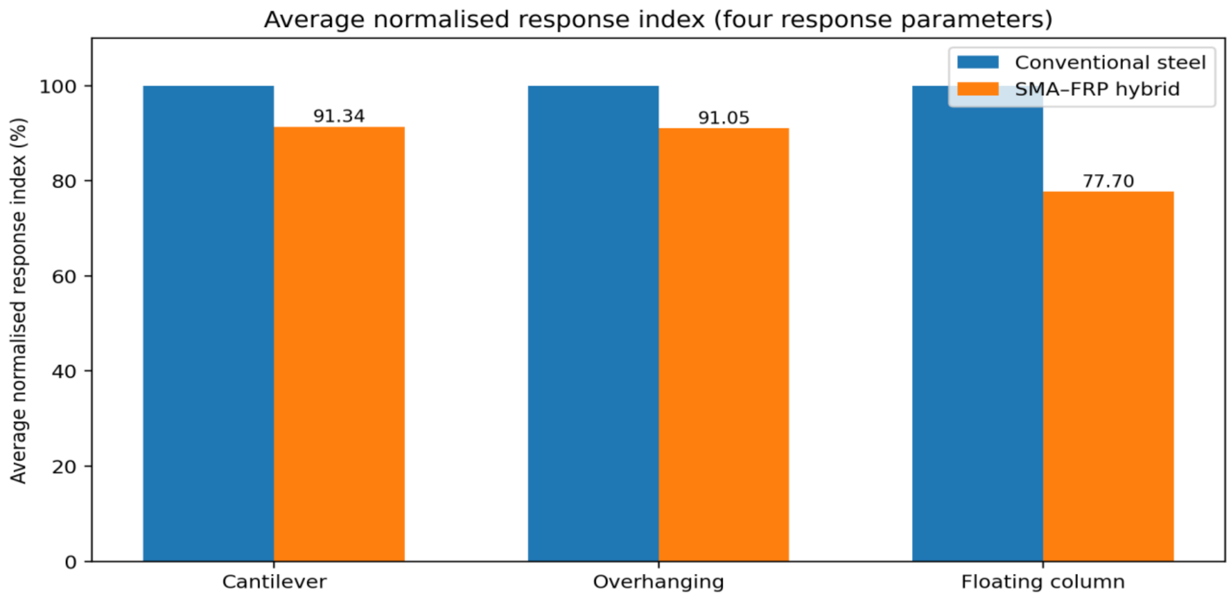

Figure 9. Average normalised response index computed from deformation, von Mises stress, elastic strain and strain energy.

Table 9. Case-wise percentage improvement and ranking.

Case	Deformation	von Mises stress	Elastic strain	Strain energy	Mean reduction	Overall interpretation
Cantilever	9.18%	8.44%	8.88%	8.15%	8.66%	Moderate, consistent improvement
Overhanging	9.21%	8.33%	9.14%	9.11%	8.95%	Moderate, consistent improvement
Floating column	20.17%	28.93%	20.02%	20.07%	22.30%	Largest benefit; still the most critical case

8.5 Engineering interpretation and comparison with published studies

The reduction in deformation and elastic strain is compatible with the general objective of limiting joint demand and improving post-event serviceability. The magnitude of improvement in the cantilever and overhanging cases is moderate, whereas the floating-column improvement is substantial. This pattern suggests that the benefit of hybrid reinforcement may become more pronounced in highly concentrated demand zones. Similar configuration sensitivity is reported in experimental literature: Pei et al. (2022) found that SMA alone did not guarantee superior stiffness, while appropriately combined SMA and steel components produced a more balanced response. Javan et al. (2023) likewise observed that partial hybridisation was more effective than complete replacement by GFRP.

The nearly unchanged principal stress requires careful interpretation. Hybrid reinforcement can alter stiffness and force transfer, causing local tensile or compressive stress components to shift even when overall deformation and von Mises stress decrease. Such redistribution is not necessarily harmful, but it must be examined against concrete cracking, crushing, bond and anchorage criteria. Qian et al. (2022) showed that improved self-centering can coexist with changes in stiffness and energy dissipation, reinforcing the need for multi-parameter assessment.

The lower static strain energy in the hybrid models should be understood as lower stored elastic energy under the analysed load, not evidence of increased hysteretic energy dissipation. Cyclic energy dissipation is the enclosed area of a load–displacement hysteresis loop. The presentation does not provide such loops, unloading branches, residual deformation or equivalent viscous damping. Therefore, the literature-supported potential of SMA–FRP systems to enhance recentering and cyclic resilience (Billah & Alam, 2012; Zafar & Andrawes, 2015; Al Ekkawi & El-Hacha, 2025) is discussed as a plausible mechanism rather than a directly demonstrated result of the present static dataset.

The floating-column findings have immediate design significance. A large percentage reduction does not eliminate the underlying irregularity. Transfer beams and joints should be designed for amplified force demand, capacity-protected against brittle shear failure and integrated with continuous lateral-force-resisting elements wherever possible. Hybrid reinforcement may be targeted to the transfer/joint region, but it should complement—not replace—sound global load-path design, ductile detailing and avoidance of abrupt stiffness/strength discontinuities.

IX. VALIDATION

9.1 Arithmetic validation of percentage differences

Each percentage was independently recalculated using Equation (3). Rounding differences are below 0.01 percentage point relative to the values displayed in the presentation. This confirms the internal arithmetic of the three case tables and invalidates the contradictory hidden conclusion that claimed 31–33% superiority of conventional steel.

Table 10. Representative arithmetic validation of reported percentage changes.

Check	Calculation	Recomputed	Presented	Rounding difference
Cantilever deformation	(4.3209−3.9244)/4.3209×100	9.1763%	9.18%	0.0037 percentage point
Cantilever von Mises stress	(143.29−131.20)/143.29×100	8.4374%	8.44%	0.0026 percentage point
Overhanging deformation	(7.7588−7.0444)/7.7588×100	9.2076%	9.21%	0.0024 percentage point
Overhanging strain energy	(9307.3−8459.7)/9307.3×100	9.1068%	9.11%	0.0032 percentage point
Floating-column deformation	(20.77−16.58)/20.77×100	20.1733%	20.18%	0.0067 percentage point
Floating-column von Mises stress	(196.38−139.57)/196.38×100	28.9286%	28.93%	0.0014 percentage point

9.2 Literature-consistency validation

The direction of the reported improvements is broadly consistent with studies in which hybrid SMA/FRP or SMA/composite systems reduced residual response, improved collapse safety or enhanced strength and recentering (Billah & Alam, 2012; Zafar & Andrawes, 2015; Nahar et al., 2020; Al Ekkawi & El-Hacha, 2025). The modest 8–9% response reductions in regular cantilever and overhanging configurations are also plausible because hybrid systems frequently trade initial stiffness against recoverability. The larger reduction in the floating-column case is physically possible where reinforcement changes significantly influence a concentrated transfer zone, but it requires confirmation using identical mesh, load and section equivalence.

A complete numerical validation cannot be performed from the presentation alone. At minimum, publication-grade verification should include: (i) a mesh-convergence study; (ii) reaction-force equilibrium; (iii) concrete cracking/crushing and reinforcement stress–strain histories; (iv) comparison with hand-calculated elastic deflection for a simplified case; (v) cyclic load–displacement hysteresis and residual deformation; and (vi) experimental or benchmark-model correlation. Agreement can only be called acceptable after those items demonstrate that the numerical response is insensitive to discretisation and reproduces a known physical response.

X. KEY FINDINGS

- The SMA–FRP model produced lower deformation, von Mises stress, elastic strain and strain energy than the conventional-steel model in all three cases.
- Cantilever deformation decreased from 4.3209 to 3.9244 mm (9.18%), while equivalent stress decreased by 8.44%.
- Overhanging-beam deformation, equivalent stress, elastic strain and strain energy decreased by 9.21%, 8.33%, 9.14% and 9.11%, respectively.
- The floating-column case was the most critical, with conventional deformation of 20.77 mm, equivalent stress of 196.38 MPa and strain energy of 37,645 mJ.
- The greatest hybrid benefit occurred in the floating-column case: 20.17% lower deformation and 28.93% lower equivalent stress.
- Middle principal stress was nearly unchanged: it increased by 0.61% in the cantilever, increased by 0.39% in the overhanging case and decreased by only 0.04% in the floating-column case.
- The mean reduction across four principal responses was 8.66% for the cantilever, 8.95% for the overhanging case and 22.30% for the floating column.
- The static results indicate response control but do not directly prove self-centering, residual-drift reduction or hysteretic energy dissipation.
- A hidden statement favouring conventional steel by 31–33% is numerically inconsistent and was rejected during the data audit.
- Hybrid reinforcement is most rationally targeted to critical hinge, joint and transfer zones as part of an integrated ductile load-path strategy.

XI. CONCLUSION

A case-wise three-dimensional finite-element comparison was undertaken for conventional steel and SMA–FRP hybrid reinforcement in cantilever, overhanging and floating-column RC configurations. The hybrid system consistently reduced the four principal static response indicators considered. For the cantilever, reductions were 9.18% in total deformation, 8.44% in equivalent stress, 8.88% in elastic strain and 8.15% in strain energy. The overhanging case exhibited comparable reductions of 8.33–9.21%. The floating-column model was the best-performing case in terms of relative hybrid improvement, with deformation reduced by 20.17%, equivalent stress by 28.93%, elastic strain by 20.02% and strain energy by 20.07%. It nevertheless remained the most demanding structural configuration because of the discontinuous vertical load path and concentration of forces in the transfer region. Middle principal stress varied by less than 0.61% in all cases, indicating local redistribution rather than a uniform decrease in every stress component. The results therefore support selective use of SMA–FRP hybrid reinforcement at critical joint, hinge and discontinuity zones where controlling response demand and improving recoverability are priorities. However, the study does not yet establish full seismic superiority because cyclic hysteresis, residual deformation, bond–slip, concrete damage variables, mesh convergence and experimental validation were not provided. The numerical evidence should consequently be viewed as a strong comparative screening result and a basis for a subsequent experimentally validated cyclic investigation.

XII. LIMITATIONS

- The complete beam and column cross-sections, cover, stirrup detailing, joint reinforcement and anchorage lengths are not reported.
- Load magnitude, axial-load ratio, loading direction, cyclic protocol and earthquake input are absent from the available numerical results.
- ANSYS element types, rebar–concrete interaction, contact settings, solver controls, mesh size and convergence study are not documented.

- The exact SMA–FRP composition, volume fractions and stress–strain curve selected from the reported material ranges are unclear.
- Only scalar maxima and contour screenshots are available; nodal histories, reaction forces, crack patterns, concrete damage and reinforcement stresses are not supplied.
- Static strain energy is reported, so cyclic energy dissipation, damping and self-centering cannot be directly quantified.
- No physical specimens or independent software/analytical model were supplied for full validation.
- The study covers three idealised configurations and cannot be generalised to complete multi-storey buildings without global system analysis.

XIII. FUTURE SCOPE

- Perform displacement-controlled reversed cyclic analysis with a standard drift protocol and report hysteresis, stiffness degradation, equivalent damping and residual deformation.
- Fabricate conventional and SMA–FRP beam–column subassemblies for quasi-static cyclic testing and calibrate the ANSYS concrete, bond and superelastic material models.
- Conduct mesh-convergence, sensitivity and uncertainty analyses for element size, bond–slip, concrete tensile strength, axial-load ratio and SMA transformation stresses.
- Investigate several SMA/FRP volume fractions and reinforcement locations to identify a cost-effective balance of initial stiffness, strength, ductility and recentering.
- Extend the analysis to full RC frames with response-spectrum, nonlinear time-history, pushover and incremental dynamic analyses under near-fault and mainshock–aftershock records.
- Evaluate durability under corrosion, moisture, temperature, fire, fatigue and ultraviolet exposure, including FRP resin degradation and SMA prestress/phase-stability effects.
- Develop design-oriented joint shear, anchorage and transfer-zone provisions and compare the hybrid solution with CFRP jacketing, steel jacketing, ECC/UHPFRC and conventional ductile detailing.
- Use multi-objective optimisation to minimise residual drift, peak deformation, stress concentration, embodied carbon and life-cycle cost while satisfying constructability constraints.

Data Availability and Editorial Note

The numerical values and images analysed in this manuscript were extracted from the supplied PowerPoint presentation. Raw ANSYS project files and solver outputs were not available. The manuscript deliberately retains all traceable values, identifies unsupported or contradictory statements and does not generate replacement numerical data. Author names, affiliations, funding, conflicts of interest and ethical declarations should be confirmed before journal submission.

REFERENCES

[1] Al Ekkawi, A., & El-Hacha, R. (2025). Experimental investigation on seismically deficient RC bridge columns strengthened with prestressed vertical Fe-SMA plates and confined with CFRP wraps and UHPFRC jacket. Engineering Structures, 332, 120010. https://doi.org/10.1016/j.engstruct.2025.120010

[2] Abraik, E. (2020). Seismic performance of shape memory alloy reinforced concrete moment frames under sequential seismic hazard. Structures, 26, 311–326. https://doi.org/10.1016/j.istruc.2020.04.025

[3] Al-Rousan, R. Z., Nusier, O. K., Abdalla, K. M., & Alhassan, M. (2023). Cyclic behavior of FRP strengthened beam-column joints under various concrete damage levels. Construction Materials, 3(1), 38–61. https://doi.org/10.3390/constrmater3010004

[4] Billah, A. H. M. M., & Alam, M. S. (2012). Seismic performance of concrete columns reinforced with hybrid shape memory alloy (SMA) and fiber reinforced polymer (FRP) bars. Construction and Building Materials, 28(1), 730–742. https://doi.org/10.1016/j.conbuildmat.2011.10.020

[5] Gao, P., Yuan, D., Chen, Z., Mosallam, A. S., Chen, T., & Wang, M. (2023). Seismic performance of RC square columns strengthened by bidirectional basalt-fiber-reinforced polymer composite laminates with fan-shaped anchors.

Construction and Building Materials, 406, 133349. https://doi.org/10.1016/j.conbuildmat.2023.133349

[6] Golias, E., Touratzidis, P., & Karayannis, C. G. (2024). Seismic response of RC beam-column joints strengthened with FRP ropes, using 3D finite element: Verification with real scale tests. CivilEng, 5(2), 395–419. https://doi.org/10.3390/civileng5020020

[7] Hashemi, S. M., & Riahi, H. T. (2022). Seismic performance of reinforced concrete beam-column joints strengthened with NSM steel bars and NSM CFRP strips. Structures, 39, 57–69. https://doi.org/10.1016/j.istruc.2022.02.072

[8] Javan, D., Kheyroddin, A., Dabiri, H., & Esfahani, M. R. (2023). Performance of RC beam-column joints with hybrid GFRP-steel reinforcement under cyclic and axial loads. Structures, 47, 1408–1415. https://doi.org/10.1016/j.istruc.2022.11.141

[9] Kabir, M. R., Alam, M. S., Said, A. M., & Ayad, A. (2016). Performance of hybrid reinforced concrete beam column joint: A critical review. Fibers, 4(2), 13. https://doi.org/10.3390/fib4020013

[10] Karayannis, C. G., & Golias, E. (2022). Full-scale experimental testing of RC beam-column joints strengthened using CFRP ropes as external reinforcement. Engineering Structures, 250, 113305. https://doi.org/10.1016/j.engstruct.2021.113305

[11] Nahar, M., Islam, K., & Billah, A. H. M. M. (2020). Seismic collapse safety assessment of concrete beam-column joints reinforced with different types of shape memory alloy rebars. Journal of Building Engineering, 29, 101106. https://doi.org/10.1016/j.jobe.2019.101106

[12] Ong, C.-B., Chin, C.-L., Ma, C.-K., Tan, J.-Y., Awang, A. Z., & Omar, W. (2022). Seismic retrofit of reinforced concrete beam-column joints using various confinement techniques: A review. Structures, 42, 221–243. https://doi.org/10.1016/j.istruc.2022.05.114

[13] Pei, Q., Wu, C., Cheng, Z., Ding, Y., & Guo, H. (2022). The seismic performance of new self-centering beam-column joints of conventional island main buildings in nuclear power plants. Materials, 15(5), 1704. https://doi.org/10.3390/ma15051704

[14] Qian, H., Li, Z., Pei, J., Kang, L., & Li, H. (2022). Seismic performance of self-centering beam-column joints reinforced with superelastic shape memory alloy bars and engineering cementitious composites materials. Composite Structures, 294, 115782. https://doi.org/10.1016/j.compstruct.2022.115782

[15] Selim, M., Khalifa, R., Elshamy, E., & Zaghlal, M. (2024). Structural efficiency of fly-ash based concrete beam-column joint reinforced by hybrid GFRP and steel bars. Case Studies in Construction Materials, 20, e02927. https://doi.org/10.1016/j.cscm.2024.e02927

[16] Zafar, A., & Andrawes, B. (2015). Seismic behavior of SMA-FRP reinforced concrete frames under sequential seismic hazard. Engineering Structures, 98, 163–173. https://doi.org/10.1016/j.engstruct.2015.03.045